ScieRxiv

NOT PEER-REVIEWED

Research Article

Hofmeister-effect-mediated double-crosslinked hydrogels for mechano-electrical and multimodal sensing

Runxuan Long[1,2], Yali Xie[2*], Huali Yang[2], Maolin Li[2], Liang Pan[1,3*]

[1]Institute of Fundamental and Frontier Sciences, University of Electronic Science and Technology of China, Chengdu 611731, Sichuan, China.

[2]CAS Key Laboratory of Magnetic Materials and Devices, Zhejiang Province Key Laboratory of Magnetic Materials and Application Technology, Ningbo Institute of Materials Technology and Engineering, China Academy of Sciences, Ningbo 315201, Zhejiang, China.

[3]Shimmer Center, Tianfu Jiangxi Laboratory, Chengdu 641419, Sichuan, China.

Correspondence to: Prof. Liang Pan, Institute of Fundamental and Frontier Sciences, University of Electronic Science and Technology of China, Chengdu 611731, Sichuan, China. E-mail: panliang@uestc.edu.cn; Prof. Yali Xie, CAS Key Laboratory of Magnetic Materials and Devices, Zhejiang Province Key Laboratory of Magnetic Materials and Application Technology, Ningbo Institute of Materials Technology and Engineering, China Academy of Sciences, Ningbo 315201, Zhejiang, China. E-mail: xieyl@nimte.ac.cn

Received: 16 May 2026 | Approved: 01 June 2026 | Online: 01 June 2026

Abstract

Hydrogels are promising soft material platforms for tissue engineering, soft robotics, and wearable electronics; however, conventional poly(vinyl alcohol) (PVA)-based

hydrogels often suffer from insufficient mechanical robustness, limited fatigue resistance, and unstable electrical signal transmission, which restrict their practical applications in durable soft devices. Herein, inspired by the anisotropic and hierarchically entangled structure of human muscle fibers, we developed an anisotropic fibrous conductive hydrogel through the coordination of long- and short-chain polymer networks and Hofmeister-effect-mediated ionic regulation. In this design, ionic salts promoted the entanglement of polymer chain segments, while magnetic Fe_3O_4 particles served as physical crosslinking points to construct a physicochemical double-crosslinked network. Benefiting from this synergistic structure, the hydrogel exhibited excellent stretchability, with a fracture strain of 561.159% at an aspect ratio of 50:1 and achieved a conductivity of 0.111 S m^{-1}. The hydrogel-based sensor accurately detected various human motions, maintained stable performance after 3,000 loading-unloading cycles, and demonstrated good environmental tolerance. Molecular dynamics simulations further revealed that enhanced intermolecular interactions contributed to the toughening mechanism. This work provides a feasible strategy for constructing high-strength, tough, and conductive anisotropic hydrogels for flexible sensing, wearable electronics, and soft robotics.

Keywords: Conductive hydrogel, hofmeister effect, physicochemical double-crosslinking, strain sensors, multi-stimulus response

INTRODUCTION

The rapid development of flexible electronics, wearable healthcare systems, soft robotics, and human-machine interfaces has created an increasing demand for soft sensing materials that can maintain reliable electrical output under large and repeated mechanical deformation[1,2]. For physiological monitoring and human motion detection, sensing materials are expected to simultaneously exhibit high stretchability, sufficient mechanical strength, stable conductivity, and good conformability to soft and curved biological tissues[3,4]. Conventional sensors based on metals or semiconductors usually possess high conductivity, but their intrinsic rigidity, limited deformability, and

mechanical mismatch with biological tissues restrict their use in long-term wearable applications[5,6]. To overcome these limitations, stretchable sensors based on elastomeric substrates, such as polydimethylsiloxane (PDMS)[7,8] and Ecoflex[9,10], have been widely explored by incorporating conductive fillers into soft matrices. Nevertheless, these composite elastomer sensors often suffer from unstable signal transmission during repeated deformation, mainly because the limited surface functional groups and weak interfacial interactions of elastomers make it difficult to achieve a homogeneous and durable conductive network through simple mechanical mixing[11].

Conductive hydrogels have emerged as promising alternatives for soft electronic devices because of their tissue-like softness, high water content, adjustable mechanical properties, and favorable biocompatibility[12]. Their three-dimensional polymer networks provide abundant functional groups and tunable crosslinking sites, which are beneficial for constructing continuous conductive pathways and improving the stability of functional components[13,14]. These features make conductive hydrogels particularly attractive for wearable strain sensors, flexible bioelectronics, and soft human-machine interfaces. In practical applications, however, soft sensors are usually attached to highly deformable and curved body surfaces, such as joints, the neck, and facial muscles, where strains can exceed 50% during daily movement[15]. Therefore, hydrogel sensors must retain both structural integrity and sensing reliability under complex mechanical deformation, repeated loading, and variable environmental conditions[16-19].

Despite considerable progress, a fundamental challenge remains in the design of conductive hydrogels: achieving mechanical robustness, electrical conductivity, and multimodal sensing capability within one material system. Many conductive hydrogels are constructed from single-network conductive polymers, including polyaniline, polypyrrole, and poly(3,4-ethylenedioxythiophene):poly(styrene sulfonate) (PEDOT:PSS)[20-22], *etc.* Although these materials can provide conductive pathways through chemical bonding, ionic crosslinking, or physical penetration, their single-network structures often lack sufficient energy dissipation mechanisms, resulting

in poor fracture resistance and limited fatigue durability. A common strategy to improve mechanical performance is to increase the crosslinking density of the hydrogel network. However, excessive crosslinking may restrict polymer chain mobility, reduce stretchability, and interfere with ion transport. Conversely, loosely crosslinked networks can preserve softness and conductivity but are prone to irreversible damage under large deformation. This trade-off between mechanical reinforcement and electrical/mechanical compliance remains a key controversy and design challenge in the field of conductive soft materials[23-25].

Double-network hydrogels offer an effective route to address this issue by combining two interpenetrating polymer networks with complementary functions. In such systems, one network can serve as a sacrificial or energy-dissipating framework, while the other maintains elasticity and structural continuity. Physical interactions, including hydrogen bonding, ionic coordination, electrostatic interactions, and crystallization domains, can further introduce reversible crosslinking sites that dissipate mechanical energy and promote self-adaptive deformation. However, many reported double-network hydrogels still rely on relatively simple network structures and are mainly designed for single-stimulus strain sensing. Their ability to integrate high mechanical toughness, stable conductivity, environmental tolerance, and multi-stimulus response remains limited. Therefore, developing a rational molecular and structural design strategy for multifunctional conductive hydrogels is essential for advancing soft materials and devices.

Biological muscle provides a useful structural inspiration for designing tough and deformable hydrogel networks. Human muscle contains hierarchically arranged fibers with different lengths and orientations, enabling efficient stress transfer, reversible deformation, and energy dissipation during movement. Inspired by this anisotropic and entangled fibrous architecture, we designed a conductive hydrogel based on long-chain poly(vinyl alcohol) (PVA) and short-chain polyethyleneimine (PEI). The combination of long and short polymer chains was expected to promote dynamic chain slippage and

hydrogen-bond-mediated energy dissipation within the hydrogel network[26]. Meanwhile, the ionic liquid 1-allyl-3-methylimidazolium bromide and inorganic salt $ZnBr_2$ were introduced to regulate intermolecular interactions through the Hofmeister effect and electrostatic interactions[27]. The presence of ionic species enhanced polymer chain entanglement and strengthened the interaction among network components. In addition, magnetic Fe_3O_4 particles were incorporated as physical crosslinking points, thereby constructing a physicochemical double-crosslinked hydrogel network.

Herein, we report a Hofmeister-effect-mediated anisotropic conductive hydrogel with enhanced mechano-electrical properties for human motion perception and multi-stimulus response. By integrating long-short polymer chain coordination, ionic regulation, and magnetic-particle-assisted physical crosslinking, the hydrogel achieved high stretchability, stable conductivity, and reliable sensing performance. The prepared hydrogel exhibited a fracture strain of 561.159% at an aspect ratio of 50:1 and a conductivity of 0.111 S m^{-1}. The corresponding hydrogel sensor accurately detected various human motions, including hand, elbow, leg, and facial movements, and maintained stable performance after repeated cycling and under low-temperature conditions. Molecular dynamics simulations were further used to clarify the changes in intermolecular interactions and reveal the toughening mechanism of the hydrogel network. These results demonstrate that the proposed physicochemical double-crosslinking strategy is effective for constructing high-strength, tough, conductive, and multifunctional hydrogels, providing a promising material platform for flexible sensing, wearable electronics, and soft robotic systems.

RESULT AND DISCUSSION

Design and fabrication of multi-stimulus responsive hydrogel structures

Long-chain PVA with high mechanical strength was selected as the main chain of the polymer network. Polyethyleneimine (PEI), as a short-chain polymer, forms a dynamic network through hydrogen bonding. Based on this, the mobility of the chain can be enhanced, and internal friction can be reduced, thereby allowing more excellent

stretchability[26,28]. We introduced ionic liquids and inorganic salts to solve the problem of device failure performance degradation caused by water evaporation during long-term use of traditional hydrogels, which we used to construct crystal domains and ionic cross-linking[29]. On the one hand, the ionic liquid 1-allyl-3-methylimidazolium bromide ([Amim]Br) can provide ionic conductivity. Since [Amim]Br can affect the intermolecular hydrogen bonds of the matrix, it will also increase the swelling and flexibility of the PVA/PEI hydrogel. Reducing the interaction between PVA chains and PEI chains, giving the material better flexibility and processability[30], At the same time, it can act as a plasticizer to a certain extent, lowering the glass transition temperature of the PVA/PEI composite material [Figures 5], thereby improving the flexibility and ductility of the material, making it perform better in applications with low temperature or high flexibility requirements[31]; On the other hand, Zn^{2+} ions can form with the hydroxyl groups on the PVA molecular chain and the amino groups on the PEI chain Cross-linking points enhance the mechanical strength and stability of the material. This cross-linking effect can significantly improve the toughness, tensile strength, and creep resistance of the composite material. IL and inorganic salts can trigger the salting out of PVA polymers that are sensitive to the Hofmeister effect, causing the polymer chains to spontaneously collapse, and during the salting out process, through electrostatic attraction, lead to strong aggregation and formation of polymer chains. Partially crystallized[32,33]. Finally, Fe_3O_4 nanoparticles are introduced to give the hydrogel magnetic response properties and serve as physical cross-linking points.

The preparation process is shown in Figure 1. A uniform mixed solution of PVA and PEI is prepared, followed by adding IL and $ZnBr_2$. After stirring evenly, magnetic Fe_3O_4 is added, and the uniformly mixed precursor solution is poured into a mold. The mixture is frozen and thawed three times at -20 °C to obtain the desired hydrogel device. First, we screened the best ratio by comparing the mechanical properties of PVA : PEI hydrogels with different ratios. As the amount of PEI increased, the fluidity between the molecular chains inside the hydrogel increased and the stretchability improved, but too much PEI would cause local short chain agglomeration and local stretchability to deteriorate.

Finally, we chose the ratio of PVA : PEI = 2 : 1 because it has the best mechanical properties (see supporting material Figures 1). The optimal amount of magnetic particles was screened. A small amount had little effect on the performance of the system, but too much addition would cause the sedimentation of the hydrogel during the freeze-thaw process to be unevenly distributed in the system or even agglomerate [Figures 2]. At the same time, the water retention capacity and stretchability decreased during subsequent use [Figures 3]. Therefore, we finally chose an amount of 50 wt% relative to PVA. The amount of PEI and Fe_3O_4 added in the subsequent hydrogels was based on this. The prepared hydrogels were freeze-dried and liquid nitrogen brittle fractured, and the cross-sectional morphology of PVA, PVA/PEI (PP), PVA/PEI/IL (PPIL), PVA/PEI/IL/$ZnBr_2$ (PPILZn), and PVA/PEI/IL/$ZnBr_2$/Fe_3O_4 (PPILZnFe) was characterized, as shown in Figure 1. It can be found that the cross-section of pure PVA hydrogel is relatively flat, and the cross-section after blending with PEI has a blocky morphology and presents a certain direction of orientation, which may be related to the orientation of water molecules during the gradual solidification process during the freeze-thaw process. After the addition of ionic liquid and $ZnBr_2$, a wrinkled morphology appeared on the cross section of the hydrogel, indicating the strong aggregation caused by the entanglement and aggregation of polymer molecular chains under the Hofmeister effect. The mapping diagram [Figures 4] shows the uniform distribution of each element, and it can also be seen that the Zn and Br elements are enriched in the wrinkled area.

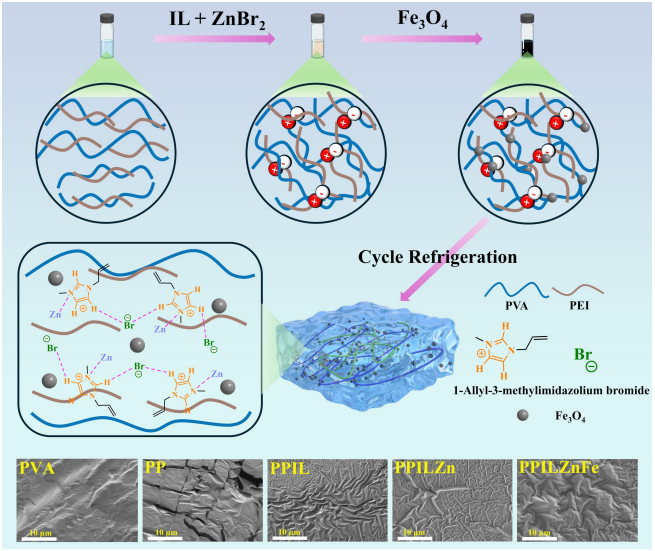

Figure 1. Flow chart of the preparation of PPILZnFe hydrogel devices, internal cross-linking network and chemical bonding, and cross-sectional SEM images of PVA, PP, PPIL, PPILZn, and PPILZnFe hydrogel devices at the bottom.

From the XRD spectrum of Figure 2 (a), it can be seen that pure PVA has a broad peak at about 20°. This broad peak corresponds to the amorphous structural characteristics of PVA, indicating that there is a certain degree of disordered arrangement between PVA molecular chains after freezing and thawing, which belongs to the semi-crystalline state[34]; the peak of PVA/PEI becomes sharper, and the amine group of PEI can form hydrogen bonds with the hydroxyl groups in the PVA molecules. These hydrogen bonds may stabilize the molecular arrangement in certain areas, thereby enhancing the local order. At the same time, the addition of PEI may lead to increased movement of PVA molecular segments, affecting the flexibility and mobility of the PVA chain. This change can make it easier for some PVA segments to arrange into a locally ordered structure, thereby slightly increasing the crystallinity; after adding ionic liquids and $ZnBr_2$, the peak intensity weakened and the peak became flat. The possible reason is that the entanglement between PVA molecular chains caused by the Hofmeister effect leads to a decrease in crystallinity, which increases the amorphous characteristics of the system[35]; finally, after adding Fe_3O_4, the corresponding characteristic peak can also be found in the spectrum (JC-PDF 97-007-7591)[36].

Furthermore, we characterized the changes in functional groups between different systems by FT-IR, as shown in Figure 2 (b). The peak at around 3,276.96 cm^{-1} in PVA is related to the stretching vibration of adsorbed water in the hydrogel and -OH in PVA; the absorption peaks at 2,917.42 cm^{-1} and 2,936.41 cm^{-1} in PP are attributed to the symmetric and antisymmetric vibrations of methylene in PVA and PEI, the peak at 1,417.98 cm^{-1} is related to the second stretching vibration of -OH, and the peak at 1,090.27 cm^{-1} belongs to C-O stretching vibration; In PP, the peaks at 1650.57 cm^{-1} and 1,569.93 cm^{-1} are related to the N-H bending vibration of amine ($-NH_2$) or secondary amine (-NH-), and the enhanced peak reflects the interaction between PEI and PVA and its molecular environment; The peak at 1,094.42 cm^{-1} belongs to C-O or C-N stretching vibration. The introduction of PEI brings a large number of amine groups ($-NH_2$) and secondary amine groups (-NH-). These amine groups can interact with the C-O bonds of PVA through hydrogen bonds, which enhances the vibrations related to C-O and C-N bonds in the FT-IR spectrum, which is a typical feature of the blending system; the enhanced peak at 847.67 cm^{-1} may be due to the fact that when PEI (polyethyleneimine) is added to the PVA matrix, the amino and imine groups in PEI may interact with the PVA molecular chain through hydrogen bonds or van der Waals forces, and this interaction may enhance the C-H vibration mode of PVA; In PPIL, The enhanced peak at 1,569.95 cm^{-1} can be attributed to the synergy of C = C and C-N stretching vibrations of the imidazole ring in IL; the presence of IL and $ZnBr_2$ may change the molecular environment of the PVA/PEI matrix through electrostatic attraction or hydrogen bond enhancement effect, causing the stretching vibration frequencies of C-O and C-N bonds to shift slightly upward, resulting in a new vibration peak at 1,166 cm^{-1}; the peak at 755.98 cm^{-1} is mainly caused by the C-H in-plane bending vibration of the imidazole ring; the peak at 847.67 cm^{-1} belongs to Br^-[37]; In PPILZn, the peak at 622.95 cm^{-1} belongs to the stretching vibration peak of Zn-Br, and the peak at 418.95 cm^{-1} belongs to the low-frequency absorption peak of $ZnBr_2$; the characteristic peak at 567.59 cm^{-1} belonging to Fe_3O_4 can also be observed in PPILZnFe[38].

Figure 2(c) is the XPS spectrum of the hydrogel. In the C spectrum, the peak at 283.91 eV in PVA is mainly C-C bond, and the peak at 285.33 eV is mainly C-O bond; the introduction of PEI adds a new C-N bond at 287.31 eV; after the addition of ionic liquid, the peak at 284.92 eV is mainly C-O bond and C = C bond coupling, and the peak intensity increases; at the same time, the introduction of ionic liquid and $ZnBr_2$ changes the ion environment, causes the electron cloud density to change, and the bond positions become cheaper to a certain extent. The peak at 398.92 eV of PVA/PEI in the N spectrum is mainly C-N bond. Amino group ($-NH_2$) or imino group (-NH-) can combine with proton (H^+) to form protonated nitrogen. Protonated nitrogen atoms usually show higher binding energy in XPS because of their positive charge. Therefore, the peak at 400.65 eV is mainly N^+-H bond. After adding ionic liquid, the N+-H bond peak is enhanced. After adding $ZnBr_2$, the newly added peak at 398.65 eV is mainly N^+-Zn^{2+} bond generated by the chelation of the amino group and Zn^{2+}. In the O spectrum, the peak at 531.07 eV of PVA is mainly C-OH bond; the shift of the peak position after the introduction of PEI indicates the formation of hydrogen bonds in the system. At the same time, PVA and PEI may also generate C = O bonds at 530.73 eV during the initial heating process. The peak at 531.97 eV corresponds to the NH-O bond formed by amino and hydroxyl groups; after the addition of IL, the N^+ on the imidazole ring can also form hydrogen bonds, causing the electron cloud density to change. The peak at 534.75 eV is attributed to the H-O-H bond. This peak type usually appears in water molecules or oxygen substances with higher polarity in the hydrogen bond network. The surface adsorption environment will lead to higher binding energy, indicating that the system is rich in hydrogen bond network. On the one hand, when $ZnBr_2$ is added, Zn^{2+} may change the electronic environment of oxygen atoms through weak coordination or electrostatic interaction, inducing the formation of Zn-O bonds in the hydrogel; on the other hand, when Zn^{2+} forms a chelate by coordinating with the amino group, the weak interaction between oxygen atoms and Zn^{2+} will reduce the electron density and increase the binding energy, corresponding to the peak at 532.91 eV; finally, the peak at 528.52 eV corresponds to the Fe-O bond of Fe_3O_4.

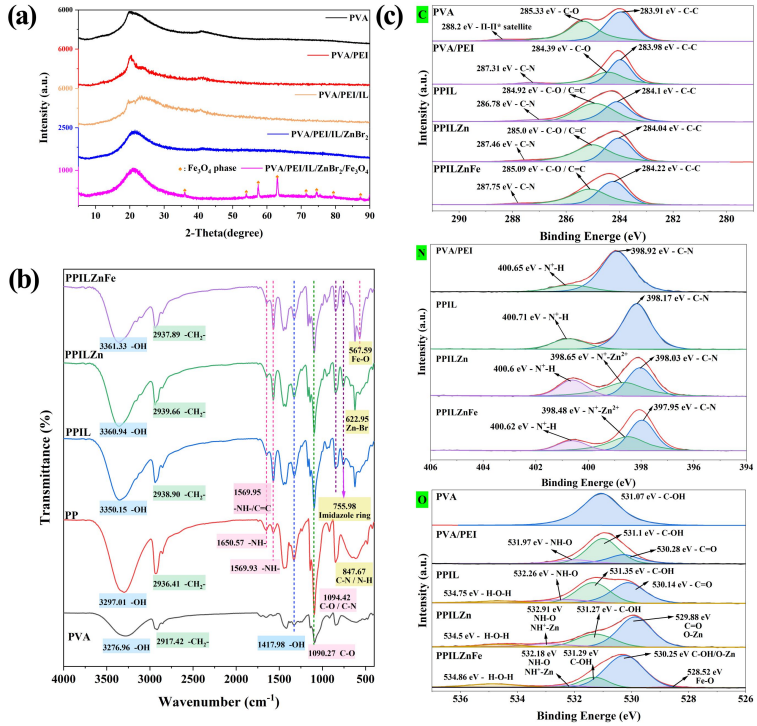

Figure 2. (a) SEM cross-sectional images of different hydrogel systems after freeze-drying; (b) Cross-sectional mapping of PPILZnFe hydrogel; (c) XRD spectra of different hydrogels; (d) FT-IR spectra of different hydrogels

Robustness and chemical properties of multi-stimulus responsive hydrogels

We tested and characterized the robustness and physical and chemical properties of the material (Test method see supporting material Text S10). The mechanical properties of PPILZnFe hydrogel were tested, Figure 3(a) tested the fracture strength of different hydrogel systems, and (b) showed the toughness and Young's modulus of different hydrogels. Traditional PVA hydrogels are based on physical cross-linking, and their breaking strain is generally about 250%, and their tensile strength is less than 300 kPa[39,40]. The introduction of PEI can enhance the internal network structure of the hydrogel through hydrogen bonding or electrostatic interaction and increase the reversible interaction between molecular chains through the coordination of long and short chains, so its tensile properties are greatly improved, reaching 323.036%, and the tensile strength also reaches 1.156 MPa; After adding IL, the hydrogel system shows higher flexibility (breaking tensile strain reaches 430.04%). Ionic liquids can increase the degree of freedom of the chain segments in the hydrogel and reduce the strong

interaction between the chain segments, resulting in the hydrogel being able to withstand greater deformation without breaking and the tensile strength reaches 1.399 MPa. The introduction of $ZnBr_2$ further enhances the reversible interaction in the hydrogel system and increases the flexibility of the hydrogel. Zn^{2+} ions can form ion-dipole interactions with hydroxyl groups in the hydrogel and can chelate with amino groups. The introduction of Br^- makes the PVA molecular chains entangled through the Hofmeister effect. The two synergistically improve the tensile strength of the system (1.799 MPa). For PPILZnFe (tensile strain 561.159%, tensile strength 1.059 MPa), the toughness increased to 4.17521 MJ/m^3. The introduction of Fe_3O_4 not only provides functionality but also serves as a physical cross-linking site for the hydrogel network during freeze-thaw. These cross-linking points enhance the stability of the system, allowing the hydrogel to provide a larger deformation space when stretched without breaking immediately. However, the decrease in tensile strength as shown in the figure may be due to the difference in the distribution of some Fe_3O_4 nanoparticles, resulting in the formation of weak interfaces or defects in the hydrogel matrix. Figure 3(c) tested the resistance change of 10 cycles under different strain conditions to determine its sensitivity. The results show that it has good linear characteristics (Support Materials Supplementary Table 1), even with continuous strain [Figures 5] still have good signal stability. In addition, the strain sensor can respond immediately to tiny stimuli, as shown in Figure 3(d), with a response time of ≈ 155 ms at 10% strain. The cyclic stability of PPILZnFe was tested, as shown in Figure 3(g); the results show that after 3,000 cycles, the electrical properties of the hydrogel still maintain excellent stability.

We tests the M-H diagram (e) and Hc diagram (f) of PPILZnFe and PPILZn after adding Fe_3O_4. PPILZn has basically no response in the field strength range of -20 kOe ~ 20 kOe. The saturation magnetization of Fe_3O_4 is 78.152 emu/g, the remanence is 7.91 emu/g, and the coercivity is -87.29 Oe. After being added to PPILZn hydrogel, the saturation magnetization of PPILZnFe hydrogel is 4.75 emu/g, the remanence is 0.447 emu/g, and the coercivity is -85.451 Oe. The curve characteristics are consistent with those of Fe_3O_4, which is a typical weak magnetic curve, indicating that it can still

respond to an external magnetic field and is expected to be used in magnetic actuation. The reason for the change in parameters is related to the shielding of the magnetic field by PPILZn hydrogel and the proportion of Fe_3O_4 in the hydrogel.

The physicochemical properties of the hydrogel were characterized to determine its toughening mechanism. Support materials Figures 6 shows the synchronous thermal analysis spectra of different hydrogels, (a) is DTG specturm, (b) is the DSC spectrum, and (c) is the TG diagram. As the system becomes more complex, the temperature change stage changes from stage 3 to stage 4 to stage 5. The mass loss within 200 °C mainly includes the loss of free water and part of the bound water. This stage also includes the glass transition of the hydrogel, and its endothermic heat gradually increases, indicating that the heat capacity of the system gradually increases. In addition to free water and bound water, it is mainly due to the increase in structural complexity (the introduction of PEI, IL, $ZnBr_2$ and Fe_3O_4 can increase the crosslinking density and enhance the intermolecular interaction); the heat release between 200 and 500 °C is mainly due to the decomposition of hydrogel molecules and ionic liquids, and the increase in the exothermic peak area is mainly due to the increase in the total amount of decomposable reactions in the system; after 500 °C, it is mainly due to the further decomposition of the ionic liquid, and the oxidation reaction of Fe_3O_4 will increase the heat release; further heating, the hydrogel molecular chain will finally break, generating volatile products such as water, carbon dioxide and other compounds.

We further evaluated the environmental tolerance of the device and tested the mechanical and electrical properties of the device by placing it at -20 ℃. Even in a low-temperature environment, the hydrogel still maintained good flexibility [Figures 7], but the device resistance increased (from 160 kΩ to 225 kΩ), which may be due to the decrease in temperature and the decrease in the ion migration rate inside the device. The device was further stretched and tested under 10% strain conditions. The results are shown in Figures 8. Compared with fresh hydrogel devices, the device can still recognize stretching at different frequencies under low temperature conditions, and the

signal sensitivity is only slightly reduced (ΔR/R (%) value is still > 90% compared with fresh devices).

We also investigated the long-term durability of the hydrogel device. After placing the hydrogel device in the external environment for 60 days, the mechanical and electrical properties of the device were tested. After 60 days, the fracture strain decreased and the tensile strength increased [Figures 9]. This may be because the water in the hydrogel will gradually evaporate when it is exposed to the external environment for a long time, resulting in a decrease in the water content inside the hydrogel. On the one hand, the reduction in water makes the hydrogel more “dry”, thereby increasing the density of the internal polymer chains, resulting in an increase in the rigidity of the material, which is manifested as an increase in tensile strength. On the other hand, water loss will reduce the flexibility of the hydrogel, making the material easier to break when stretched, resulting in a decrease in fracture strain. We conducted a cyclic stability test on the hydrogel device after 60 days of placement. As shown in Figure s 10, the device still has very good cyclic stability in 520 cycles. This proves the good prospects of PPILZnFe hydrogel devices in long-term wear test applications.

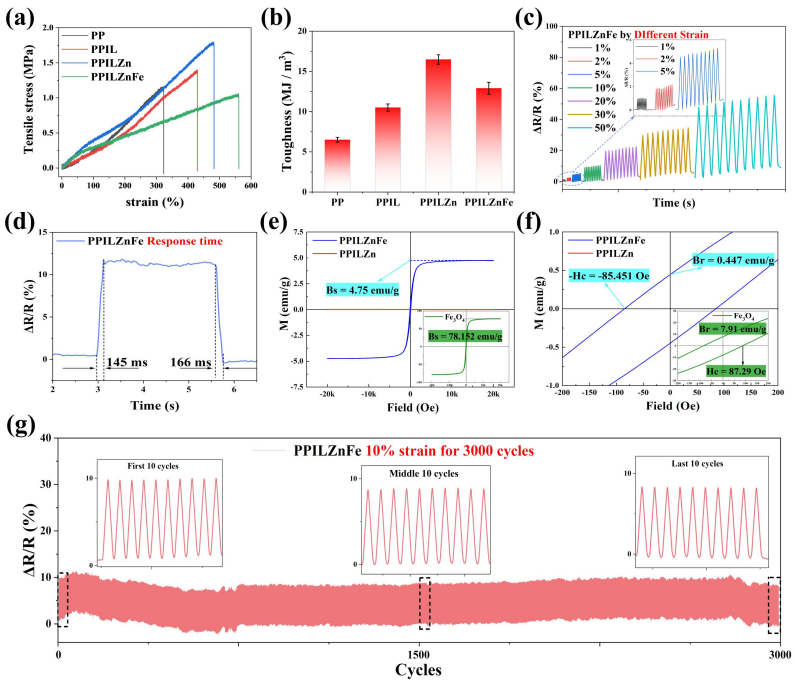

Figure 3. (a) Stress-strain curves of hydrogels of different systems; (b) Corresponding toughness and Young's modulus; (c) Signals of PPILZnFe hydrogels under cyclic stretching for 10 times under different strain conditions; Hysteresis loop (VSM) test of PPILZnFe before and after adding Fe_3O_4 (e) M-H curve and (f) HC curve; (d) Cyclic stability test of PPILZnFe (10% strain, 3,000 cycles)

Molecular dynamics simulation (MD) of physicochemical double-crosslinked hydrogels based on the Hofmeister effect

We performed molecular dynamics simulations on systems 1 (PVA/PEI) and 2 (PVA/PEI/IL/$ZnBr_2$/Fe_3O_4). By simulating molecular motion, intermolecular forces, gyration radius, radial distribution function of PVA and PEI with other molecules in system 2, and changes in coordination number, we explained the changes in the structure and stability of the hydrogel from a theoretical perspective.

Figure 4(a) shows representative snapshots of the two systems at the initial moment and after 20 ns NPT ensemble equilibrium and 10 ns stretching along the X direction. It can be seen from the snapshots that as the simulation proceeds, PVA and PEI in system 1 are more likely to form block aggregates, the molecular distribution is more aggregated,

thinner molecular chains connect the two aggregates, and after 10 ns stretching, the two aggregates break. In system 2, with the addition of IL and $ZnBr_2$, the molecular distribution of PVA and PEI is more uniform, no obvious agglomeration occurs, and obvious connecting chains are formed between molecules. After 10 ns stretching, the molecular chains still exist, indicating improved mechanical properties. Figure 4(b) calculates the two systems' interaction energy between PVA molecules and PEI molecules. The interaction energy between PVA and PEI in system 1 is stronger than in system 2, indicating that the contact between PVA and PEI in system 2 is weaker, which is conducive to the dynamic slippage between molecules during stretching[41,42]. The radius of gyration of the polymer reflects its volume and shape. The larger the radius of gyration, the fluffier the system[43]. Figure 4(c) represents the radius of gyration of the aggregates formed by PVA and PEI molecules in the two systems in the X direction during the simulation time. According to (c), it can be seen that the radius of gyration of the aggregates in system 2 is significantly larger than that in system 1, indicating that the aggregates formed by PVA and PEI molecules in system 2 are more dispersed, which helps to create more chains to enhance its mechanical properties, which is also consistent with the snapshot in (a). Figure 4(d) and (e) show the trend of the interaction energy (Coulomb (Coul) and Lennard-Jones (LJ)) between PVA and PEI and different solvent molecules (ionic liquid (IL), Zn^{2+}, Br^-) in system 2 over time[43]. It can be found that IL shows the most significant van der Waals force on PVA and PEI, indicating that PVA and PEI show significant attraction with ionic liquids, among which the van der Waals force on PVA drops to -12,000 kJ/mol, then tends to be stable, which is greater than the force on PEI (-8,000 kJ/mol), and then tends to be stable, which also indicates that the force of IL on PVA is more significant than that on PEI; the Coul (about -4,500 kJ/mol) and LJ (about -2,000 kJ/mol) of bromide ions on PVA are both strong, especially the Coulomb effect. Compared with PEI (Coul: about -1,800 kJ/mol, LJ: about -1,100 kJ/mol), the interaction between Br^- and PVA is stronger overall because the functional groups of PVA are more conducive to forming strong electrostatic attraction with negatively charged bromide ions, which is consistent with the Hofmeister effect; since the amount of Zn^{2+} in the system is small, it has little effect on

the system; Figure 4(f) (g) shows the radial distribution function G (r) and coordination number N (r) between PVA and PEI and different solvent molecules (ionic liquid (IL), Zn^{2+}, Br^-) in system 2[44,45]. The G(r) function shows that the density of IL around PVA and PEI is high, which can produce the most significant interaction force, followed by Br^-, where the density around PVA is slightly higher than that of PEI; the N(r) function shows that the coordination numbers of the PVA-IL and PEI-IL curves rise rapidly, indicating that the ionic liquid molecules can form a higher coordination around PVA and PEI molecules and produce strong local interactions, followed by Br^-, where the coordination number for PVA is slightly higher than that for PEI, which is consistent with the intermolecular forces simulated in Figure 4(d) and (e); since the amount of Zn^{2+} in the system is small, it has little effect on the system; In short, we have theoretically calculated the intermolecular forces of the system through molecular dynamics simulation and found that, on the one hand, due to the addition of IL and $ZnBr_2$, PVA and PEI have a strong attraction, which enhances the intermolecular interaction energy between the system, and on the other hand, it weakens the intermolecular forces between PVA and PEI. At the same time, the system's gyration radius increases, and the agglomerates become dispersed, which helps to form more chains to enhance its mechanical properties, consistent with the experimental data.

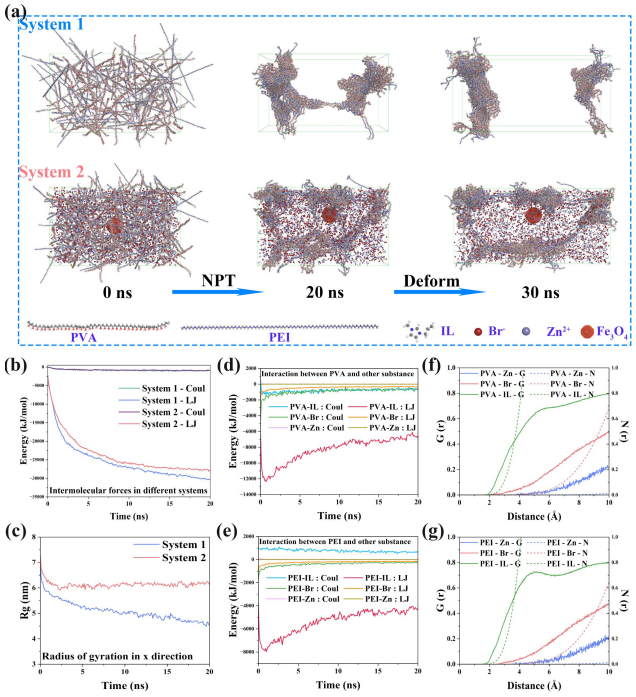

Figure 4. Results of molecular dynamics simulation calculations: system 1 : PVA/PEI, system 2 : PVA/PEI/IL/ZnBr2/Fe3O4. (a) Changes in molecular motion of system 1 and system 2; (b) Changes in intermolecular forces of systems 1 and 2; (c) Gyration radius of systems 1 and 2 in the x direction; (d) Intermolecular forces between each substance in system 2 and PVA; (e) Intermolecular forces between each substance in system 2 and PEI; (f) Radial distribution function and coordination number between PVA and other substances in system 2; (g) Radial distribution function and coordination number between PEI and other substances in system 2.

PPILZnFe hydrogels for human motion detection and environmental perception

Due to its sensitive sensing ability, PPILZnFe hydrogel can be used as a wearable sensor to monitor human activities in real time. It can sensitively identify joint movements, including fingers, elbows, and legs; the relative resistance change positively correlates with the degree of deformation. After the hydrogel is fixed on the index finger, the lifting and bending of the finger joints can be accurately monitored, and the different swing amplitudes and frequencies of the fingers can also be accurately reflected. As shown in the large figure of Figure 5(a), when the finger is lifted, the device is compressed, the device resistance decreases, and the signal shifts to a negative

value; the first joint of the finger is slightly bent, and the device can effectively identify it, and the signal changes slightly. Further bending the finger greatly increases the change in signal intensity. At the same time, the device can effectively respond to high-frequency and low-frequency bending actions; We also monitored the activity signals of the thumb, index finger, middle finger, and ring finger during the process of making and releasing a fist. As shown in the four figures below Figure 5(a), due to the different lengths of the fingers, the bending during the process of making a fist leads to different strains of the device, and the output electrical signals under the same action are significantly different, mainly reflected in the different changes in ΔR/R. Therefore, based on the signal differences on different fingers, there is a good application prospect in the mapping of human hands by manipulators. Figure 5(b) fixes the hydrogel device on the elbow joint to simulate the bending of the elbow joint during the swinging process of the human hand. Because the human skin at the elbow joint is more elastic than the finger joint, the maximum amplitude of the signal change during the bending process is close to 4 times that of the finger signal. After fixing the hydrogel device on the side of the thigh, we monitored the movement state of the volunteers. Figure 5(c) shows that the signal output is relatively stable in the walking state, and the output electrical signal changes more frequently and the signal is sharper in the running state, which can explain the movement state of the leg muscles during running. At the same time, we noticed that there is relaxation in the lowest value of the signal in the running state. This is mainly because the leg muscles are always in a tense state during running, and the device always maintains a certain stretch. In short, the experimental results show that the device can effectively monitor the walking and running state of the human body. Figure 5(d) shows the changes in electrical signals when the volunteers raised and squeezed their eyebrows after the hydrogel was fixed on the eyebrows. When squeezing the eyebrows, the muscles between the two eyes contracted, the device contracted, the resistance decreased, and the output signal tended to be negative; when raising the eyebrows, the forehead skin relaxed, causing the device to stretch and the resistance to increase. For such relatively small changes in the human eyebrows, the device also has sensitive and stable detection and recognition capabilities, making PPILZnFe hydrogel a

strong competitor for strain sensors for flexible wearable devices for full-range human motion detection. Due to the introduction of ferroferric oxide, in addition to giving the device the ability to actuate under the action of an external magnetic field, we also noticed that it responded to external infrared light (650 nm, 100 mW), as shown in Supporting Figures 11. Under infrared light irradiation, the device resistance decreased, and after turning off the light source, the resistance recovered. This may be due to the local magnetothermal effect of magnetic ferroferric oxide under infrared light irradiation. The thermal effect improves the ion transmission efficiency of the corresponding part, and the resistance of the device changes, which is then reflected in the difference in the output signal. On the other hand, the device also has a certain response to humidity changes. As shown in Supporting Figures 12, the device is fixed on a horizontal table, and the different breathing states of people are simulated by the breathing behavior of volunteers at different rates and depths. In the normal breathing state, as the gas is exhaled, the device resistance decreases. This is because during the exhalation process, the environment increases moderately, and the hydrogel device absorbs water, which increases the internal conductive path and reduces the resistance. At the same time, the device can effectively identify different exhalation states, such as short and rapid breathing and deep and long breathing, and has good application prospects for identifying human health status through breathing states in the future.

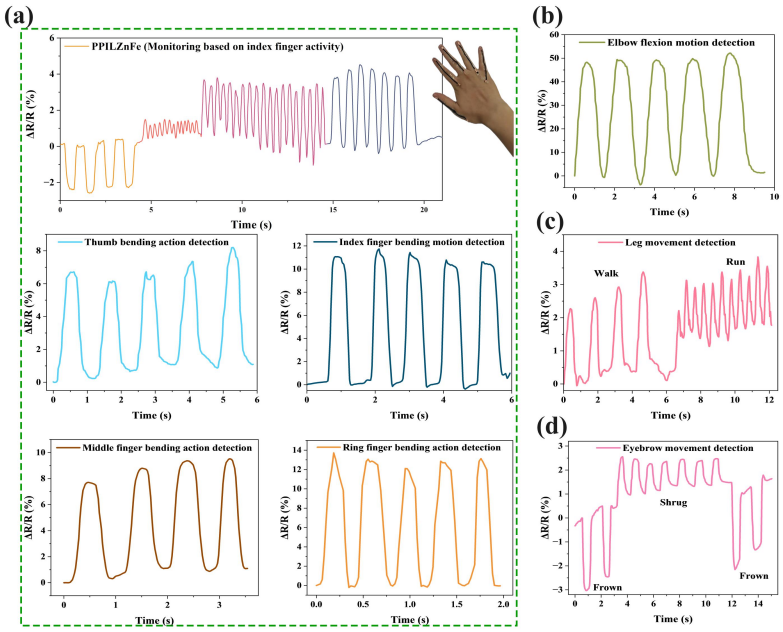

Figure 5. (a) The electrical signals of the index finger under different activity states after the hydrogel is fixed; bottom of figure, changes in electrical signals of different fingers in clenched and relaxed fist states; (b) The changes of electrical signals under elbow bending after the hydrogel is fixed on the elbow; (c) The changes of electrical signals under walking and running after the hydrogel is fixed on the leg; (d) The changes of electrical signals under eyebrow raising and eyebrow squeezing after the hydrogel is fixed on the eyebrow

CONCLUSION

In summary, inspired by the interconnected and hierarchical structure of human muscle fibers, we developed a Hofmeister-effect-mediated physicochemical double-crosslinked conductive hydrogel with enhanced mechanical, electrical, and multi-stimulus responsive properties. Long-chain PVA and short-chain PEI were combined to construct a dynamic polymer network, in which molecular chain slippage and hydrogen-bonding interactions effectively improved the stretchability and toughness of conventional PVA-based hydrogels. The incorporation of the ionic liquid 1-allyl-3-methylimidazolium bromide and $ZnBr_2$ provided ionic conductivity and promoted polymer chain entanglement through the Hofmeister effect and electrostatic interactions, thereby further strengthening the hydrogel network. Meanwhile, Fe_3O_4

particles acted as physical crosslinking sites and endowed the hydrogel with additional responsiveness to external stimuli.

Benefiting from this synergistic design, the conductive hydrogel exhibited a large fracture strain of 561.159% and an ionic conductivity of 0.111 S m^{-1} under different stretching states. The hydrogel also showed reliable sensing performance, including a good linear response, stable signal output after 3,000 loading-unloading cycles at 10% strain, and long-term stability after 60 days of storage. Moreover, the hydrogel sensor could sensitively detect finger movements even at -20 °C, demonstrating its potential for wearable sensing under low-temperature conditions. Owing to the introduction of Fe_3O_4 particles, the hydrogel further responded to external magnetic fields and infrared irradiation, indicating its capability for multi-stimulus sensing.

Characterization and theoretical calculations further revealed the interaction mechanisms among the hydrogel components, confirming that enhanced mechanical performance originated from the synergistic effects of hydrogen bonding, ionic interactions, polymer chain entanglement, and physical crosslinking. This work provides a feasible strategy for designing high-strength, stretchable, conductive, and multifunctional hydrogels, and offers a promising material platform for flexible strain sensors, human motion monitoring, wearable electronics, and soft robotic systems.

Experimental section

Experimental details are available in the Supporting Information.

DECLARATIONS

Authors' contributions

Made substantial contributions to conception and design of the study and performed data analysis and interpretation: RX.L, L.P;

Performed data acquisition, as well as provided administrative, technical, and material support: RX.L, L.P, YL.X, HL.Y, ML.L.

Availability of data and materials

Data is available on request.

Financial support and sponsorship

Zhiming Wang acknowledges support from the Nation Key Resear and Development Program of China (Grant No.2019YFB2203400) and the “111 Project” (Grant No.B20030); Liang Pan acknowledges support from the Science & Technology Department of Sichuan Province (Grant No.2024ZYD0026) and the Tianfu Jiangxi Laboratory (No.TFJX-ZD-2025-006).

Conflict of interest

The authors declare no conflict of interest.

Ethical approval and consent to participate

This study did not involve animal experiments, patient samples, clinical trials, or any invasive procedures. The on-body sensing demonstrations, if any, were performed only for non-invasive device performance evaluation. No ethical approval was required for this study.

All participants in the non-invasive body surface sensing demonstration gave their consent.

Consent for publication

The participant provided consent for the publication of the relevant experimental data and images.

Copyright

REFERENCES

1. Cheng, I.C.; Wagner, S. Overview of Flexible Electronics Technology. In *Flexible Electronics: Materials and Applications*, Wong, W.S., Salleo, A., Eds.; Springer US: Boston, MA, 2009; pp. 1-28.[DOI: 10.1007/978-0-387-74363-9_1]

2. Rogers, J.A. Materials for semiconductor devices that can bend, fold, twist, and stretch. *MRS Bulletin* **2014**, *39*, 549-56,[DOI: 10.1557/mrs.2014.102]

3. Wang, C.; Wang, C.; Huang, Z.; Xu, S. Materials and Structures toward Soft Electronics. *Advanced Materials* **2018**, *30*, 1801368,[DOI: 10.1002/adma.201801368]

4. Kim, D.-H.; Lu, N.; Ma, R.; et al., Epidermal Electronics. *Science* **2011**, *333*, 838-43,[DOI: 10.1126/science.1206157]

5. Yamada, T.; Hayamizu, Y.; Yamamoto, Y.; et al., A stretchable carbon nanotube strain sensor for human-motion detection. *Nature Nanotechnology* **2011**, *6*, 296-301,[DOI: 10.1038/nnano.2011.36]

6. Wang, Z.; Cong, Y.; Fu, J. Stretchable and tough conductive hydrogels for flexible pressure and strain sensors. *Journal of Materials Chemistry B* **2020**, *8*, 3437-59,[DOI: 10.1039/C9TB02570G]

7. Soe, H.M.; Manaf, A.A.; Matsuda, A.; Jaafar, M. Development and fabrication of highly flexible, stretchable, and sensitive strain sensor for long durability based on silver nanoparticles-polydimethylsiloxane composite. *Journal of Materials Science: Materials in Electronics* **2020**, *31*, 11897-910,[DOI: 10.1007/s10854-020-03744-6]

8. Gao, Y.; Fang, X.; Tan, J.; Lu, T.; Pan, L.; Xuan, F. Highly sensitive strain sensors based on fragmentized carbon nanotube/polydimethylsiloxane composites. *Nanotechnology* **2018**, *29*, 235501,[DOI: 10.1088/1361-6528/aab888]

9. Madhavan, R. Epidermis-Like High Performance Wearable Strain Sensor for Full-Range Monitoring of the Human Activities. *Macromolecular Materials and Engineering* **2022**, *307*, 2200034,[DOI: 10.1002/mame.202200034]

10. Okada, K.; Horii, T.; Yamaguchi, Y.; et al., Ultraconformable Capacitive Strain Sensor Utilizing Network Structure of Single-Walled Carbon Nanotubes for Wireless Body Sensing. *ACS Applied Materials & Interfaces* **2024**, *16*, 10427-38,[DOI: 10.1021/acsami.3c19320]

11. Niu, D.; Jiang, W.; Ye, G.; et al., Graphene-elastomer nanocomposites based flexible piezoresistive sensors for strain and pressure detection. *Materials Research Bulletin* **2018**, *102*, 92-9,[DOI: 10.1016/j.materresbull.2018.02.005]

12. Zhu, T.; Ni, Y.; Biesold, G.M.; et al., Recent advances in conductive hydrogels: classifications, properties, and applications. *Chemical Society Reviews* **2023**, *52*, 473-509,[DOI: 10.1039/D2CS00173J]

13. Pan, S.; Xia, M.; Li, H.; et al., ransparent, high-strength, stretchable, sensitive and anti-freezing poly(vinyl alcohol) ionic hydrogel strain sensors for human motion monitoring. *Journal of Materials Chemistry C* **2020**, *8*, 2827-37,[DOI: 10.1039/C9TC06338B]

14. Sun, J.; Xiu, K.; Wang, Z.; et al., Multifunctional wearable humidity and pressure sensors based on biocompatible graphene/bacterial cellulose bioaerogel for wireless monitoring and early warning of sleep apnea syndrome. *Nano Energy* **2023**, *108*, 108215,[DOI: 10.1016/j.nanoen.2023.108215]

15. Zhao, C.; Park, J.; Root, S.E.; Bao, Z. Skin-inspired soft bioelectronic materials, devices and systems. *Nature Reviews Bioengineering* **2024**, *2*, 671-90,[DOI: 10.1038/s44222-024-00194-1.

16. Zhang, J.; Zhang, Q.; Liu, X.; Xia, S.; Gao, Y.; Gao, G. Flexible and wearable strain sensors based on conductive hydrogels. *Journal of Polymer Science* **2022**, *60*, 2663-78,[DOI: 10.1002/pol.20210935]

17. Zhang, J.; Shen, S.; Lin, R.; et al., Highly Stretchable and Biocompatible Wrinkled Nanoclay-Composite Hydrogel With Enhanced Sensing Capability for Precise Detection of Myocardial Infarction. *Advanced Materials* **2023**, *35*, 2209497,[DOI: 10.1002/adma.202209497]

18. Wang, L.; Xu, T.; Zhang, X. Multifunctional conductive hydrogel-based flexible wearable sensors. *TrAC Trends in Analytical Chemistry* **2021**, *134*, 116130,[DOI: 10.1016/j.trac.2020.116130]

19. Liu, Y.; Wang, L.; Mi, Y.; et al., Transparent stretchable hydrogel sensors: materials, design and applications. *Journal of Materials Chemistry C* **2022**, *10*, 13351-71,[DOI: 10.1039/D2TC01104B]

20. Gao, X.; Lin, J.; Yu, C.; Tang, C.; Huang, Y. Constructing multifunctional polyvinyl alcohol composite hydrogels with human-like skin properties using polyaniline-coated boron nitride nanofibers. *European Polymer Journal* **2024**, *215*, 113238,[DOI: 10.1016/j.eurpolymj.2024.113238]

21. Pan, L.; Chortos, A.; Yu, G.; et al., An ultra-sensitive resistive pressure sensor based on hollow-sphere microstructure induced elasticity in conducting polymer film. *Nature Communications* **2014**, *5*, 3002,[DOI: 10.1038/ncomms4002]

22. Lu, B.; Yuk, H.; Lin, S.; et al., Pure PEDOT:PSS hydrogels. *Nature Communications* **2019**, *10*, 1043,[DOI: 10.1038/s41467-019-09003-5]

23. Guo, Y.; Feng, S.; Gao, W.; et al., Attapulgite-Reinforced Robust and Ionic Conductive Composite Hydrogels for Digital Light Processing 3D Printing. *Advanced Functional Materials* **2024**, *n/a*, 2408775,[DOI: 10.1002/adfm.202408775]

24. Guo, X.; Qin, W.; Gu, C.; et al., High-Adhesion, Weather Resistance, Reusable PAM/Gly/Gel/TA/Fe3+ Biopolymer Dual-Network Conductive Hydrogel for Flexible Bioelectrode. *Advanced Materials Technologies* **2024**, *9*, 2302072,[DOI: 10.1002/admt.202302072]

25. Yan, X.; Ma, Y.; Lu, Y.; et al., Zeolitic Imidazolate-Framework-Engineered Heterointerface Catalysis for the Construction of Plant-Wearable Sensors. *Advanced Materials* **2024**, *36*, 2311144,[DOI: 10.1002/adma.202311144]

26. Huang, J.; Xu, Y.; Qi, S.; et al., Ultrahigh energy-dissipation elastomers by precisely tailoring the relaxation of confined polymer fluids. *Nature Communications* **2021**, *12*, 3610,[DOI: 10.1038/s41467-021-23984-2]

27. Wan, J.; Wang, F.; Zhong, M.; Liang, Y.; Wu, J. Skin-like dual-network gelatin/chitosan/emodin organohydrogel sensors mediated by Hofmeister effect and Schiff base reaction. *International Journal of Biological Macromolecules* **2024**, *280*, 135837,[DOI: 10.1016/j.ijbiomac.2024.135837]

28. Liu, Y.; Wang, C.; Liu, Z.; et al., Self-encapsulated ionic fibers based on stress-induced adaptive phase transition for non-contact depth-of-field camouflage sensing. *Nature Communications* **2024**, *15*, 663,[DOI: 10.1038/s41467-024-44848-5]

29. Yang, X.; Xu, L.; Wang, C.; et al., Reinforcing Hydrogel by

Nonsolvent-Quenching-Facilitated In Situ Nanofibrosis. *Advanced Materials* **2023**, *35*, 2303728,[DOI: 10.1002/adma.202303728]

30. Wu, S.; Hua, M.; Alsaid, Y.; et al., Poly(vinyl alcohol) Hydrogels with Broad-Range Tunable Mechanical Properties via the Hofmeister Effect. *Advanced Materials* **2021**, *33*, 2007829,[DOI: 10.1002/adma.202007829]

31. Yu, Y.; Yang, X.; Zhang, C.; Chen, J.; Lin, W.; Meng, J. A tough double-network ion gel membrane based on poly (ionic liquid) for efficient carbon capture. *Separation and Purification Technology* **2024**, *331*, 125591,[DOI: 10.1016/j.seppur.2023.125591]

32. Li, X.; Mei, X.; Chen, M.; et al., Solvent-induced phase separation and Hofmeister effect enhanced strong, tough, and adhesive polyion complex hydrogels. *Chemical Engineering Journal* **2024**, *497*, 154673,[DOI: 10.1016/j.cej.2024.154673]

33. Zhao, W.; Zhou, H.; Li, W.; Chen, M.; Zhou, M.; Zhao, L. An Environment-Tolerant Ion-Conducting Double-Network Composite Hydrogel for High-Performance Flexible Electronic Devices. *Nano-Micro Letters* **2024**, *16*, 99,[DOI: 10.1007/s40820-023-01311-2]

34. Xu, Q.; Hou, M.; Wang, L.; Zhang, X.; Liu, L. Anti-bacterial, anti-freezing starch/ionic liquid/PVA ion-conductive hydrogel with high performance for multi-stimulation sensitive responsive sensors. *Chemical Engineering Journal* **2023**, *477*, 147065,[DOI: 10.1016/j.cej.2023.147065]

35. Ren, J.; Chen, G.; Yang, H.; et al., Super-Tough, Non-Swelling Zwitterionic Hydrogel Sensor Based on the Hofmeister Effect for Potential Motion Monitoring of Marine Animals. *Advanced Materials* **2024**, *n/a*, 2412162,[DOI: 10.1002/adma.202412162]

36. Alipour, S.; Pourjavadi, A.; Hosseini, S.H. Magnetite embedded κ-carrageenan-based double network nanocomposite hydrogel with two-way shape memory properties for flexible electronics and magnetic actuators. *Carbohydrate Polymers* **2023**, *310*, 120610,[DOI: 10.1016/j.carbpol.2023.120610]

37. Yamada, T.; Mizuno, M. Characteristic Spectroscopic Features because of Cation-Anion Interactions Observed in the 700-950 cm-1 Range of Infrared Spectroscopy for Various Imidazolium-Based Ionic Liquids. *ACS Omega* **2018**, *3*,

8027-35,[DOI: 10.1021/acsomega.8b00938]

38. Cao, Q.; Shu, Z.; et al., Magnetic nanocomposite hydrogel with ultra-stretchable as strain sensors for monitoring human motion and the change of magnetic field. *Journal of Applied Polymer Science* **2024**, *141*, e54934,[DOI: 10.1002/app.54934]

39. Dong, Y.; Gao, Z.; Mi, Q.; et al., Highly sensitive and structure stable polyvinyl alcohol hydrogel sensor with tailored free water fraction and multiple networks by reinforcement of conductive nanocellulose. *International Journal of Biological Macromolecules* **2024**, 136128,[DOI: 10.1016/j.ijbiomac.2024.136128]

40. Chen, K.; Liang, K.; Liu, H.; et al., Skin-Inspired Ultra-Tough Supramolecular Multifunctional Hydrogel Electronic Skin for Human-Machine Interaction. *Nano-Micro Letters* **2023**, *15*, 102,[DOI: 10.1007/s40820-023-01084-8]

41. Jia, L.; Jiang, J.; Ren, A.; Wei, Z.; Xiang, T.; Zhou, S. Ultra-fast cryogenic self-healing ionic hydrogel for flexible wearable bioelectronics. *Chemical Engineering Journal* **2024**, *495*, 153734,[DOI: 10.1016/j.cej.2024.153734]

42. Es Sayed, J.; Mukherjee, A.; El Aani, S.; et al., Structure-Property Relationships of Granular Hybrid Hydrogels Formed through Polyelectrolyte Complexation. *Macromolecules* **2024**, *57*, 3190-201,[DOI: 10.1021/acs.macromol.3c02335]

43. Liu, J.F.; GhavamiNejad, A.; Lu, B.; Mirzaie, S.; Samarikhalaj, M.; Giacca, A.; Wu, X.Y. “Smart” Matrix Microneedle Patch Made of Self-Crosslinkable and Multifunctional Polymers for Delivering Insulin On-Demand. *Advanced Science* **2023**, *10*, 2303665,[DOI: 10.1002/advs.202303665]

44. Zhao, Y.; Chen, C.; Zhu, Z.; et al., Hofmeister effect driven dynamic-bond cross-linked dialdehyde xylan hydrogels with rapid response and robust mechanical properties for expanding stent. *International Journal of Biological Macromolecules* **2024**, *280*, 135888,[DOI: 10.1016/j.ijbiomac.2024.135888]

45. Wang, F.; Yu, X.; Cao, Z.; Liu, Y.; Jiang, X.; Gu, X. Synergic enhancement of hydrogel upon multi-level hydrogen bonds via macromolecular design for dual-mode electronic skin. *Chemical Engineering Journal* **2024**, *489*, 151249,[DOI: 10.1016/j.cej.2024.151249]